Structural and magnetic phase transitions in Fe - I boracite, $Fe_3B_7O_{13}I$

1997 J. Phys.: Condens. Matter 9 2607

(http://iopscience.iop.org/0953-8984/9/12/009)

J. Phys.: Condens. Matter **9** (1997) 2607–2621. Printed in the UK PII: S0953-8984(97)76504-4

Structural and magnetic phase transitions in Fe–I boracite, $Fe_3B_7O_{13}I$

Z-G Ye†§, A-M Janner‡§ and H Schmid§

† Department of Chemistry and Chemical Engineering, Faculty of Engineering, Niigata University, Niigata 950-21, Japan

‡ Laboratory of Solid State Physics, Materials Science Centre, University of Groningen, Nijenborgh 4, NL-9747 AG Groningen, The Netherlands

§ Department of Inorganic, Analytical and Applied Chemistry, University of Geneva, CH-1211 Geneva 4, Switzerland

Received 19 July 1996

Abstract. The structural and magnetic phase transitions of Fe–I boracite have been studied by means of optical examinations of the domain structure and by measurements of the spontaneous birefringence using polarized-light microscopy. These phase transitions have also been characterized by dielectric and spontaneous polarization studies, realized on ferroelastic/ferroelectric single-domain states, which were obtained by electric field poling along $\langle 100\rangle_{cub}$ and $\langle 111\rangle_{cub}$ directions, with simultaneous visual control of the domain state. In the trigonal $3m1'$ phase, an electric field $\boldsymbol{E}\|\langle 111\rangle_{cub}$ of one polarity produced a monodomain with the spontaneous polarization $\boldsymbol{P}_s$ and the optical axis perpendicular to the $(111)_{cub}$ plane, while that of the reversed polarity gave rise to domains with the three other preferential directions of $\boldsymbol{P}_s$, non-collinear with $\boldsymbol{E}$, and to a polarization of $\boldsymbol{P}_s/3$, indicating the non-180°-reversibility of $\boldsymbol{P}_s$ along $\langle 111\rangle_{cub}$. The magnetic phase transition $3m1' \leftrightarrow m$ resulted in anomalies both in the dielectric permittivity (up to 2 MHz) and in the spontaneous polarization at the Curie temperature $T_C = 31$ K. This suggests an interaction between the magnetic moment and the electric polarization, consistent with the ferroelectric/ferroelastic/ferromagnetic coupling effect previously found for the *m* phase.

1. Introduction

The crystal family of boracites has the general formula $M_3B_7O_{13}X$ (M–X), where M stands for divalent metal ions (Mg, Cr, Mn, Fe, Co, Ni, Cu, Zn, or Cd) and X for halogen ions (F, Cl, Br or I), with more than 20 isomorphous compounds. They each have a cubic paraelectric and diamagnetic or paramagnetic high-temperature phase of space group $F\bar{4}3c1'$ (Shubnikov point group $\bar{4}3m1'$). Upon cooling most (but not all) of the boracite crystals present a phase transition from the cubic prototype phase to a fully ferroelectric/fully ferroelastic $mm21'$ phase, or to a sequence of phases with the point groups $mm21'$, $m1'$ and $3m1'$ [1–5]. The boracites containing the paramagnetic 3d-transition-metal ions of Fe, Co, Ni, Cu, Cr or Mn are particularly interesting because they undergo phase transitions into magnetically ordered states at low temperatures, becoming therefore simultaneously ferroelectric/ferroelastic and weakly ferromagnetic, i.e, multi-ferroic [1, 6], permitting both linear and bilinear magnetoelectric effects.

Upon cooling, the boracite $Fe_3B_7O_{13}I$ (abbreviated as Fe–I) shows a sequence of structural phase transitions from the cubic $\bar{4}3m1'$ to the orthorhombic $mm21'$, the monoclinic

0953-8984/97/122607+15$19.50

$m1'$, and the trigonal $3m1'$ phases, as established by optical domain studies [4], x-ray diffraction [7], and Mössbauer spectroscopy [8, 9]. This sequence includes all of the non-magnetic phases disclosed up to now in the boracites, except the tetragonal $\bar{4}2m1'$ phase, which has only been observed in Cr–Cl [10]. At low temperature an essentially antiferromagnetic order appears below the Curie temperature $T_C \approx 30$ K, as revealed by magnetic neutron reflections [11]. A weak ferromagnetic moment was measured from magnetic hysteresis loops [12].

In a recent study, the magnetic phase transition $3m1' \leftrightarrow m$ at $T_C = 30(\pm 1)$ K was studied by means of optical domain analysis and measurements of the spontaneous birefringence [13]. However, the results so far published on the structural phase transitions of Fe–I showed some incoherent points, especially concerning the temperatures of the $mm21' \leftarrow T_2 \rightarrow m1' \leftarrow T_3 \rightarrow 3m1'$ transitions. An unusually strong thermal hysteresis was reported from the temperature dependence of the lattice parameters as determined by single-crystal x-ray diffraction: upon cooling and heating, $T_2 = 203$ and 218 K, and $T_3 = 191$ and 205 K, respectively [7]. Such a thermal hysteresis would indicate an overlap of phases between 191 and 218 K. The characterization of the physical properties of Fe–I, such as the dielectric constant, pyroelectricity and spontaneous polarization [14–16], optical properties [4, 17, 18], latent lattice strain [19], and crystal structure [20], was mainly carried out in the orthorhombic $mm21'$ phase and for the ferroelectric/paraelectric phase transition near 345 K.

In this work the structural and magnetic phase transitions in Fe–I have been investigated in detail by means of optical domain examination, and dielectric and polarization measurements, in order to establish the phase sequence and to study the effects on the dielectric permittivity and the spontaneous polarization induced by the magnetic phase transition.

2. Experimental procedure

Fe–I boracite single crystals were grown by the chemical-vapour-transport technique [21, 22]. Platelets of different thicknesses (20 to 50 μm) were cut parallel to $(100)_{cub}$, $(110)_{cub}$ and $(111)_{cub}$ and finely polished. Some of the $(100)_{cub}$ and $(111)_{cub}$ cuts were electroded by deposition of semi-transparent Au–Cr layers, which permit a simultaneous optical control of the domain states during both the poling and the characterizing processes. Samples were mounted on a rotating rod in an optical He-flow cryostat (8 to 300 K), specially adapted to a polarized-light microscope. The dielectric properties were characterized using an Impedance Analyzer (HP4192A). The value and the relative change of the dielectric permittivity are very small at low temperatures, leading to a variation of the measured parallel capacitance of $\Delta C_p = 10^{-3}$ pF (see section 4). The use of a compensating capacitance was necessary to measure ΔC_p within the digital limit of the apparatus. The spontaneous polarization was measured with an electrometer (Keithley 616) by charge integration. The birefringence was measured with a tilting compensator M.

3. Optical domain structures and phase transitions

3.1. The domain structure of the $mm21'$ phase

At room temperature, the Fe–I crystals present an orthorhombic phase with point group $mm21'$. The domain structure of the $mm2$ phase consists of six fully ferroelastic/fully ferroelectric domains which are totally coupled, consistent with the ferroic species

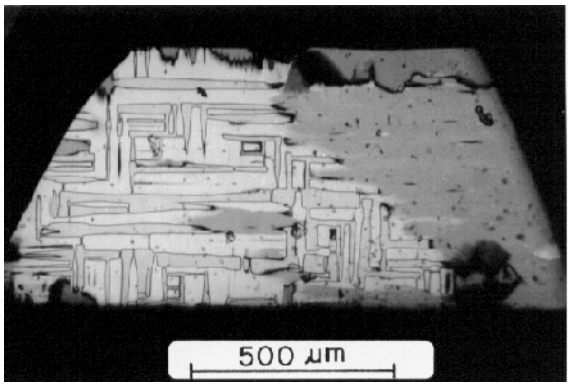

(a)

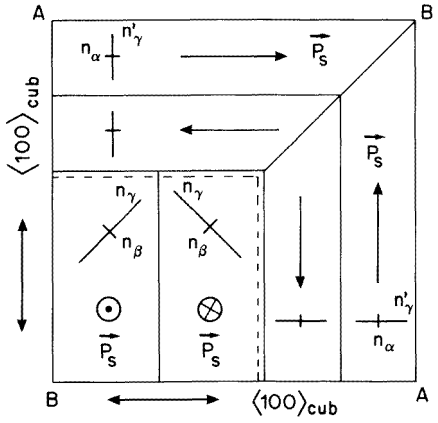

(b)

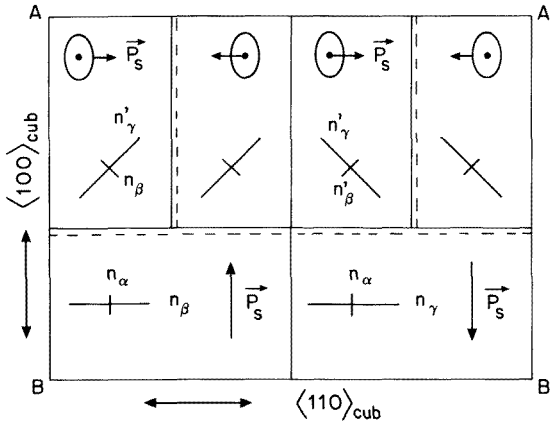

(c)

Figure 1. (a) A photograph showing the domain pattern of the orthorhombic $mm21'$ phase of Fe–I boracite on a $(100)_{cub}$ platelet (thickness = 37 μm, T = 293 K); (b) a schematic representation of the six orthorhombic ferroelectric/ferroelastic domains with sections of birefringence on $(100)_{cub}$ planes; (c) a schematic representation of the $mm21'$ domain state on $(110)_{cub}$ cuts.

$\bar{4}3m1'Fmm21'$ [23]. Figures 1(a) and 1(b) give the observed domain structure and the schematic pattern for a $(100)_{cub}$ platelet with the spontaneous polarization parallel to the six $\langle 001\rangle_{cub}$ directions. In agreement with the previous notation [4], the optical indicatrix of the orthorhombic phase is found to be of type B, i.e. with the principal indices n_α parallel to $\boldsymbol{P}_s \| [001]_{or}$ ($\| [001]_{cub}$), n_β and n_γ parallel to $[100]_{or}$ and $[010]_{or}$ (i.e. $\| \langle 110\rangle_{cub}$), respectively, and with the optical axes lying in the orthorhombic b, c-plane. Therefore, one of the principal birefringences, $\Delta n_{\gamma\beta}$, can be identified on $(100)_{cub}$ planes (figure 1(b)), and the other two, $\Delta n_{\gamma\alpha}$ and $\Delta n_{\beta\alpha}$, can be identified on $(110)_{cub}$ cuts (figure 1(c)). Measurements on crystals of different thicknesses (18 to 35 μm) provide the mean values $\Delta n_{\gamma\alpha} = 4.7 \times 10^{-3}$ and $\Delta n_{\gamma\beta} = 3.9 \times 10^{-3}$ at 293 K ($\lambda = 542$ nm). The value of $\Delta n_{\gamma\alpha}$ is lower than the one given previously ($\Delta n_{\gamma\alpha} = 6.3 \times 10^{-3}$, $\Delta n_{\gamma\beta} = 4.0 \times 10^{-3}$ and $\Delta n_{\beta\alpha} = 2.1 \times 10^{-3}$) [4], suggesting that the $(110)_{cub}$ platelets studied may contain a superposition of domains partially compensating the birefringence $\Delta n_{\gamma\alpha}$.

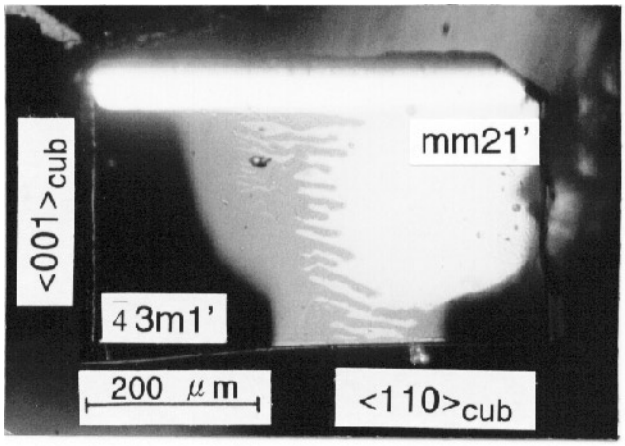

Figure 2. The domain pattern showing the presence of an intermediate grey state on a $(110)_{cub}$ platelet (35 μm thick, with a growth sector on the top) between the cubic phase and the initial $(n_\gamma - n_\alpha)$ orthorhombic domains during the $\bar{4}3m1' \leftrightarrow mm21'$ phase transition at 347 K.

3.2. The $mm21' \leftrightarrow \bar{4}3m1'$ phase transition

Upon heating, the Fe–I crystals undergo a phase transition from the orthorhombic $mm21'$ phase to the cubic $\bar{4}3m1'$ phase with the disappearance of the birefringent domains. The phase transition monitored by optical domain transformation on various $(100)_{cub}$, $(110)_{cub}$ and $(111)_{cub}$ cuts upon heating and cooling takes place over a large temperature interval in which the cubic and the orthorhombic phases coexist. Upon heating, the cubic phase appears at about $T_1 = 336$ K while the orthorhombic phase disappears completely only at 349 K; upon cooling, the $mm21'$ phase appears at 348 K whereas the $\bar{4}3m1'$ phase subsists down to 336 K (at 1 K min^{-1}). The thermal hysteresis indicates the first-order character of the phase transition. The large temperature interval would result from the presence of different growth sectors (pyramids), which may show huge differences in the ferroelectric phase transition temperature with non-uniform phase transition, as observed previously in boracite crystal plates [24].

Figure 2 shows the domain state of a $(110)_{cub}$ platelet at the $\bar{4}3m1' \leftrightarrow mm21'$ transition, where a grey state with weak birefringence appears between the cubic phase and the initial

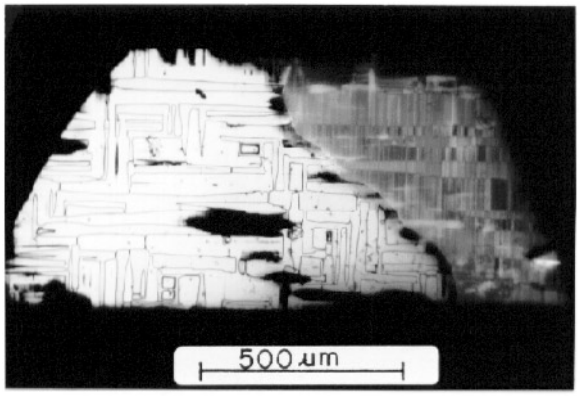

(a)

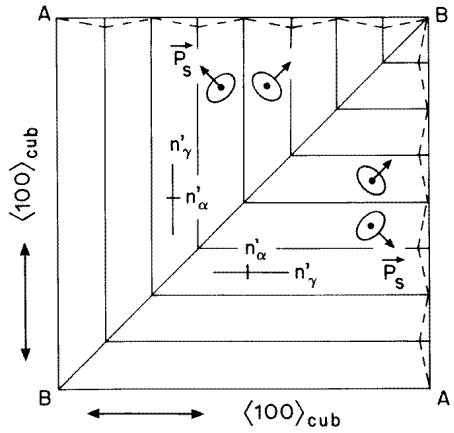

(b)

Figure 3. The domain structure of the monoclinic $m1'$ phase: (a) a photograph of a $(100)_{cub}$ platelet (thickness = 37 μm, $T = 186$ K) with the formation of packages of lamellar domains, especially inside the orthorhombic domains with $\boldsymbol{P}_s$ lying in the plane of the platelet (see figures 1(a) and 1(b)); (b) a schematic view of the splitting up of the head–head and tail–tail domains into lamellae with their composition planes perpendicular to the orthorhombic $\boldsymbol{P}_s$.

orthorhombic $\Delta n_{\gamma\alpha}$ domains, separating the isotropic area from the birefringent domains of the $mm21'$ phase. Such an intermediate state remains pinned to the cubic phase boundary and propagates through the crystal during the cubic/orthorhombic phase transition. For the $mm21' \rightarrow \bar{4}3m1'$ phase transition, the grey state can coexist with the cubic phase and replace all of the initial $\Delta n_{\gamma\alpha}$ domains on $(110)_{cub}$ planes. On $(100)_{cub}$ planes, the grey state appears in the form of lamellae with weaker birefringence. The birefringence of the grey state and the temperature at which it appears increase with the decreasing thickness of the platelets: on $(110)_{cub}$, $\Delta n = 1.20 \times 10^{-3}$ at 339 K for a thickness of 35 μm while $\Delta n = 1.78 \times 10^{-3}$ at 347 K for a thickness of 13 μm. This apparent thickness dependence of the birefringence suggests the presence of superimposed domains. The appearance of the grey state during the $mm21' \leftrightarrow \bar{4}3m1'$ phase transition may therefore result from the formation of fine layers with cubic symmetry inside the $mm21'$ domains. Another reason for the occurrence of the grey state may be the changes in the direction of the spontaneous

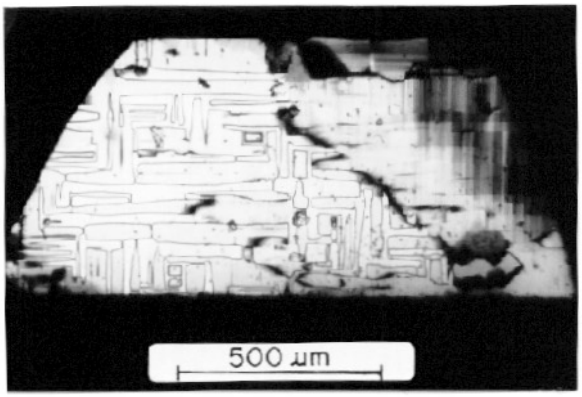

(a)

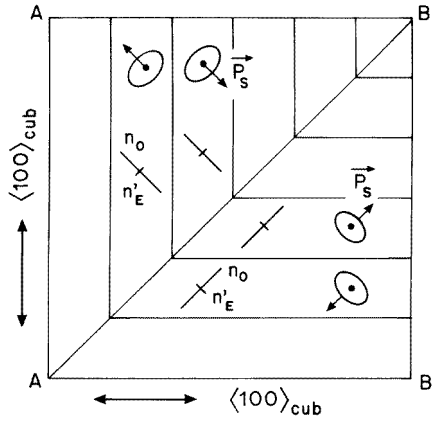

(b)

Figure 4. The domain structure of the trigonal $3m1'$ phase: (a) a photograph of the $(100)_{cub}$ platelet ($T = 148$ K) with a slightly modified lamellar structure; (b) a schematic representation of the domain orientation of the trigonal lamellae.

polarization of the $mm2$ phase during the phase transition. As indicated in figure 1(c), on a $(110)_{cub}$ cut, a 180° reversal of $\boldsymbol{P}_s$ interchanges the domains with birefringence $\Delta n_{\gamma\alpha}$ and $\Delta n_{\beta\alpha}$. The birefringence value of the grey layer is close to $\Delta n_{\beta\alpha}$. This would mean that on $(110)_{cub}$ platelets, when the cubic phase is present, the domains of $\Delta n_{\beta\alpha}$ with weaker birefringence become more stable than the domains of $\Delta n_{\gamma\alpha}$, probably due to a mechanical mismatching at the phase boundary. On $(100)_{cub}$ platelets, the grey lamellae would result from the appearance of the domain states with $\boldsymbol{P}_s$ in the planes (figure 1(b)).

3.3. The $mm21' \leftrightarrow m1' \leftrightarrow 3m1'$ phase transitions

Upon cooling, the orthorhombic phase transforms into a monoclinic $m1'$ phase at $T_2 \approx$ 200 K. The $mm21' \rightarrow m1'$ transition can be characterized by the splitting up of a $mm21'$ domain state into a package of very fine lamellar domains, with their composition plane perpendicular to the former $mm2$ polar direction, as schematically explained by figure 3(b). The formation of this lamellar twin is due to an attempt of the crystal to minimize the

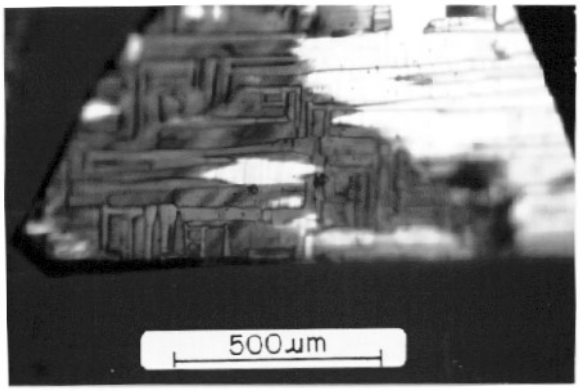

Figure 5. Stripes of sub-domains revealed by inclining the $(100)_{cub}$ platelet in the trigonal $3m1'$ phase.

mechanical and electrostatic energy of the system. This domain structure results in twelve orientation states, consistent with the species $\bar{4}3m1'Fm1'$ [23]. On $(100)_{cub}$ platelets, these lamellar domains appear inside those orthorhombic domains which have the spontaneous polarization lying in the plane and the birefringence $(n_{\gamma'} - n_{\alpha})$, as formerly observed for other boracites with the $mm21' \rightarrow m1'$ transition (reference [4], figures 18 and 20). The $mm21'$ domains with $\boldsymbol{P}_s$ perpendicular to the plane of the platelets remain almost unchanged (figure 3). Indeed, the monoclinic domain splitting is not observable along the direction of the orthorhombic polarization, because the domains are finely superposed and they keep the same orientation of the optical indicatrix section, giving rise to a very small difference in birefringence values between the $mm21'$ and the $m1'$ phase. This difference may almost vanish along special crystallographic orientations, as in the case of $\Delta n_{\beta\alpha}$ for Fe–Cl boracite [4].

Upon further cooling below 190 K the lamellae tend to fade away, giving rise to more stable, larger grey domains with nevertheless some subsisting fine domains. At the transition to the $3m1'$ phase at $T_3 \approx 180$ K, the packages of very fine rhombohedral lamellar domains appear with an orientation of the composition planes that is the same as that of the previous monoclinic domains (figure 4). The species $\bar{4}3m1'F3m1'$ allows four ferroelectric/ferroelastic domains with the spontaneous polarization along the four tetrahedral non-reversible polar $\langle 111 \rangle_{cub}$ directions, and the section of principal birefringence lying on a $(110)_{cub}$ plane. The domains with $\boldsymbol{P}_s$ perpendicular to the $(100)_{cub}$ planes remain apparently unchanged, but some contrasted sub-domains in stripe form are observed when inclining the platelet (figure 5).

These phase transitions are also observed on $(110)_{cub}$ and $(111)_{cub}$ cuts but with less clarity, because of irregular extinctions due to a highly superimposed domain structure.

3.4. The magnetic phase transition $3m1' \rightarrow m$

It has been shown that the magnetic phase transition from the trigonal $3m1'$ to a monoclinic m phase at $T_C = 30(\pm 1)$ K resulted in the ferroelastic domain splitting and the appearance of linear birefringence on the originally rhombohedral $(111)_{cub}$ section, due to a magneto-structural deformation with monoclinic symmetry [13]. One trigonal single domain splits up into three ferroelectric/ferroelastic domains and 3×2 ferromagnetic domains with anti-

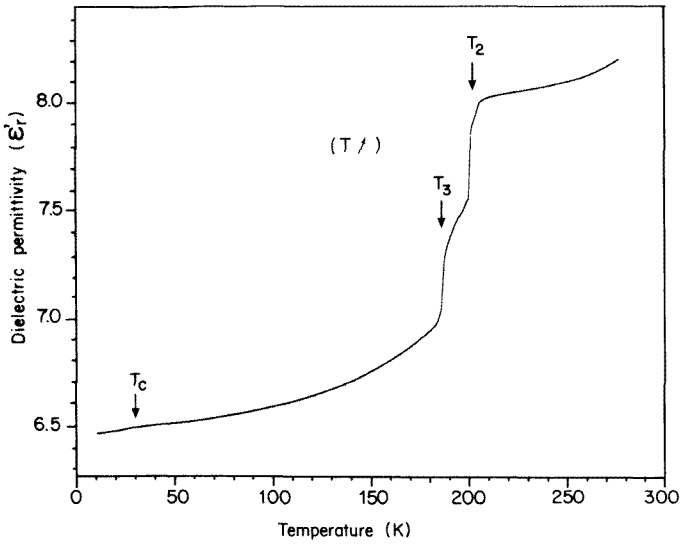

(a)

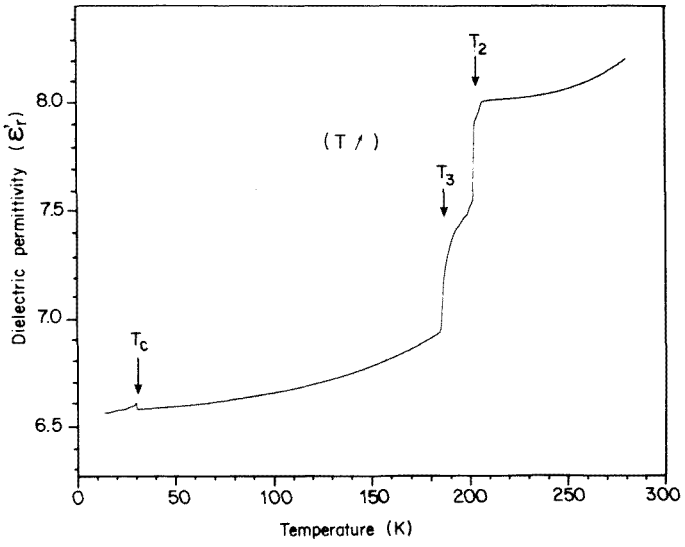

(b)

Figure 6. Temperature dependences of the real parts of the dielectric permittivities of a $(111)_{cub}$ Fe–I platelet (thickness = 20 μm, $f = 1$ MHz) measured upon heating from: (a) a poled trigonal $3m1'$ single-domain state; (b) an unpoled $3m1'$ polydomain state with a clearer anomaly at the magnetic phase transition at $T_C = 30$ K.

parallel spontaneous magnetization $\boldsymbol{M}_s$ perpendicular to the three $(110)_{cub}$ planes (mirror m). These ferromagnetoelastic domains can be switched by the action of a magnet, giving rise to spontaneous current and charge pulses as a result of ferromagnetic, ferroelectric and ferroelastic couplings. The domain orientations are consistent with the Aizu species $\bar{4}3m1'Fm$ which allows a total of 12×2 partially ferromagnetic/fully ferroelectric/fully

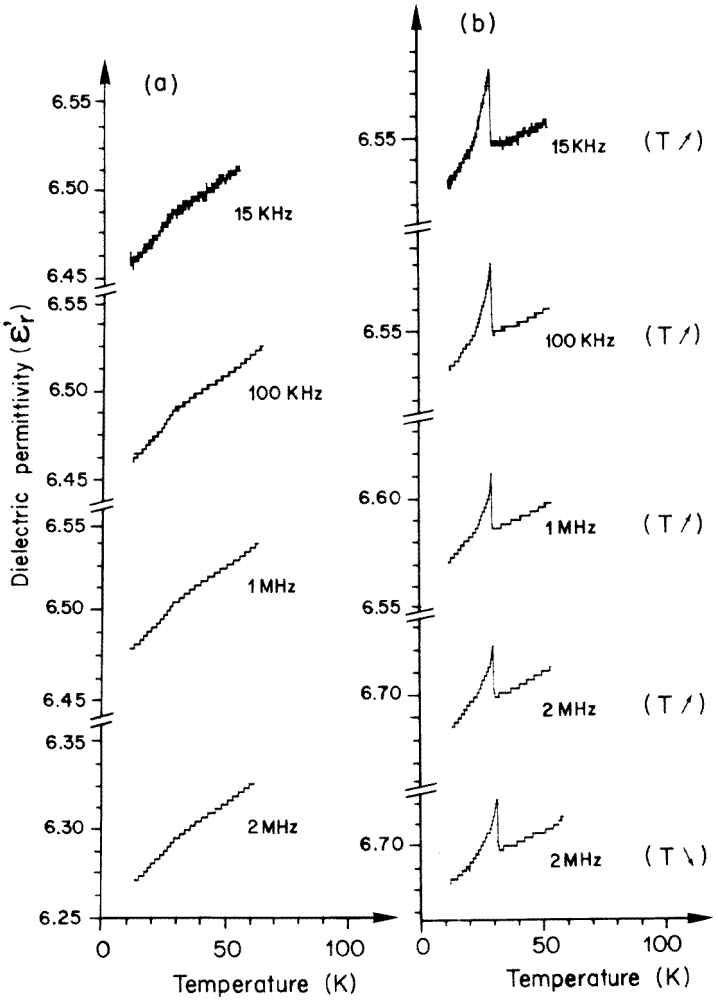

Figure 7. Details of the magnetically induced dielectric anomaly at various frequencies from: (a) a poled trigonal $3m1'$ single-domain state; (b) an unpoled $3m1'$ polydomain state.

ferroelastic orientation states [23]. This domain structure is also applicable to other magnetic boracites undergoing the $3m1' \rightarrow m$ phase transition, such as Co–Cl ($T_C = 10$ K) [5, 25, 26], Fe–Cl ($T_C = 10.5$ K) [12] and Fe–Br ($T_C = 18$ K [12], 18.4 K [9]).

4. Dielectric characterization

The dielectric properties of Fe–I crystals were studied as a function of temperature and frequency. The temperature dependence of the real part of the permittivity ε_r' measured at 1 MHz upon heating on a $(111)_{cub}$ platelet is shown in figure 6(a) for a single-domain state and in figure 6(b) for a polydomain state of the $3m1'$ phase. The trigonal single-domain state with spontaneous polarization perpendicular to the $(111)_{cub}$ planes was obtained by poling with an electric field of 100 kV cm^{-1} along $\langle 111 \rangle_{cub}$, as described in a previous publication [13]. The phase transitions $mm21' \leftrightarrow m1'$ at T_2 and $m1' \leftrightarrow 3m1'$ at T_3 are clearly

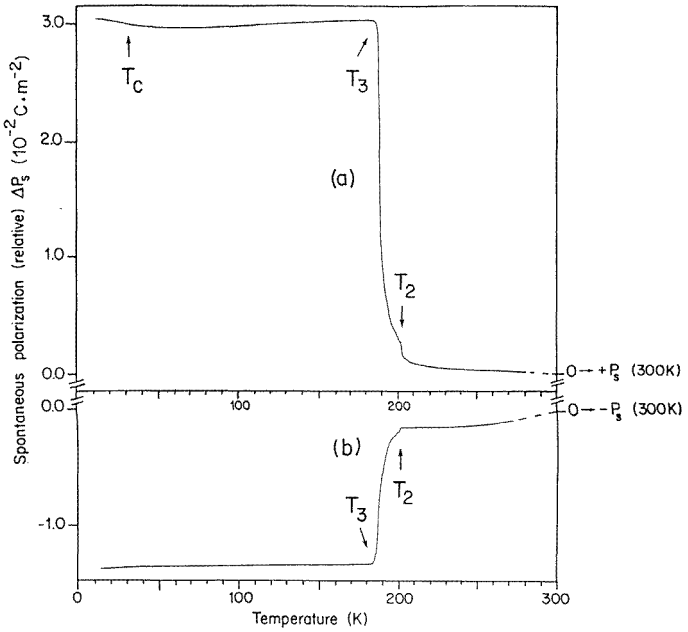

Figure 8. Asymmetric curves of the temperature dependence of the spontaneous polarization measured on the $(111)_{cub}$ Fe–I platelet from: (a) a trigonal single-domain state obtained with a poling field $\boldsymbol{E} \| \boldsymbol{P}_s \| [111]_{cub}$; (b) a polydomain state with the three other domains with inclined $\boldsymbol{P}_s$ for the reversed polarity of the poling field.

revealed by the discontinuities of the dielectric constant, indicating a first-order character for these structural phase transitions in Fe–I. The small shoulder above T_2 results from a rearrangement of the monoclinic domains, as observed by simultaneous visual control. A comparison between figures 6(a) and 6(b) shows that the variation of $\varepsilon_r'(T)$ in the $3m1'$, $m1'$ and $mm21'$ phases and at the structural phase transitions is nearly independent of the initial domain structure of the trigonal $3m1'$ phase. Therefore the dielectric permittivity presents a weak anisotropy.

The magnetic phase transition at $T_C = 31$ K affects the dielectric properties, giving rise to a slight second-order change of slope of the $\varepsilon_r'(T)$ curve in the case of an initial trigonal single-domain state (figure 6(a)) and to a peak of ε_r' in the case of a polydomain state (figure 6(b)). These magnetically induced dielectric anomalies measured with higher resolution at various frequencies are shown in figures 7(a) and 7(b) for a trigonal single-domain and a polydomain state, respectively.

The sharp peak of the dielectric constant at the magnetic phase transition can be attributed to a contribution of electric charges generated at the ferroic domain walls. As explained in section 3.4, each ferroelectric/ferroelastic $3m1'$ domain splits into six ferroelectric/ferroelastic/ferromagnetic monoclinic domains. A trigonal polydomain (unpoled) state generates all of the 24 multi-ferroic domains in the *m* phase. The appearance (or disappearance) of the ferroelectric/ferroelastic magnetic domains and the associated motion of walls at T_C necessarily lead to the formation of electric charges at the domain walls, since the magnetic easy direction is coupled to the ferroelectric/ferroelastic orientation states. These charges in turn respond to the external exciting field and thereby contribute to the permittivity, giving rise to a dielectric anomaly at T_C. It can be seen from figure 7(b)

that the dielectric peak decreases with increasing frequency while T_C remains unchanged, which agrees with the mechanism of domain wall charge contribution. In the case of a poled trigonal single-domain state, the number of ferroic domains below T_C is reduced by a factor of 4, i.e. from 24 to 6, and they appear with a large size (up to 30 μm edges) [13]. Consequently the effect of charges from the ferroelectric domain walls is quite attenuated, and the parasitic dielectric anomaly becomes less visible.

5. Spontaneous polarization

The spontaneous polarization of Fe–I has been measured upon heating in the m, $3m1'$, $m1'$ and $mm21'$ phases between 10 and 270 K. Figure 8 shows the temperature dependence of the relative variation of the polarization on a $(111)_{cub}$ platelet with respect to its value for the orthorhombic phase at room temperature, which was previously determined to be $\boldsymbol{P}_s = 3.7 \times 10^{-2}$ C m^{-2} ($\boldsymbol{P}_s \| \langle 001 \rangle_{cub}$) [14]. The upper curve (a) refers to a poled trigonal single-domain state with spontaneous polarization perpendicular to the $(111)_{cub}$ plane of the platelet ($\boldsymbol{P}_s \| \boldsymbol{E} \| [111]_{cub}$). The lower curve (b) corresponds to a trigonal three-domain state with $\boldsymbol{P}_s$ inclined, obtained by a poling field of reversed polarity, as discussed in reference [13].

The asymmetric behaviour of the polarization, with respect to opposite electric field polarity, can be ascribed to the fact that the $\langle 111 \rangle_{cub}$ directions in the prototype $\bar{4}3m1'$ phase are already polar owing to the boron–oxygen net, forbidding a 180° reversal of the spontaneous polarization in the trigonal phase. Poling with a field polarity ($E >$ 100 kV cm^{-1}) parallel to one of the four trigonal polar axes results in a single-domain state of the trigonal $3m1'$ phase, with the spontaneous polarization and the optical axis perpendicular to the $(111)_{cub}$ platelet. The measured value corresponds, therefore, to the trigonal polarization $\boldsymbol{P}_s$ (figure 8(a)). On reversing the field polarity (figure 8(b)), the single domain splits up into three possible trigonal domain states with their $\boldsymbol{P}_s$ and the optical axis inclined at about 35° to the $(111)_{cub}$ surface [13]. The polarization value measured on $(111)_{cub}$ represents in reality a projection of $\boldsymbol{P}_s$ with a value of $P_s/3$. The experimental data are close to but slightly higher than this ratio. This is due to the presence of some domains with $\boldsymbol{P}_s$ inclined which usually subsist in the 'single-domain' state, probably blocked by some defects or by scratches due to polishing, reducing the measured value of $\boldsymbol{P}_s$.

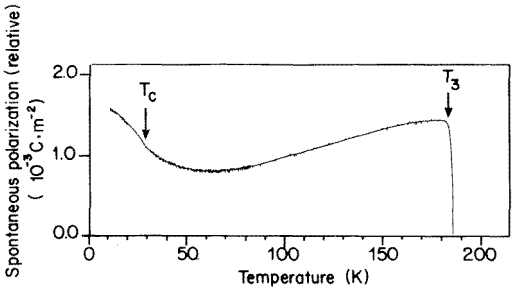

Figure 9. Detail of the $\boldsymbol{P}_s$–T variation showing a slight decrease of the spontaneous polarization below T_3, an increase below 60 K, and a change of slope at the magnetic phase transition temperature T_C. The small peaks are due to noise.

The structural phase transitions at T_2 and T_3 are revealed by the discontinuous variation of the polarization, in agreement with the dielectric properties. Below T_3, the polarization

decreases slightly and shows a broad minimum at around 60 K (figure 9). This behaviour is also present in other boracites, e.g. in the orthorhombic $mm21'$ phases of Cr–Cl [27], Ni–Br [29] and Mg–Cl [29] and in the trigonal $3m1'$ phase of Co–Cl boracite [25, 26]. A phenomenological analysis using Landau theory has been undertaken to interpret the properties of the spontaneous polarization in the orthorhombic boracites [30]. A similar analysis is applicable to the trigonal boracite of Fe–I, too.

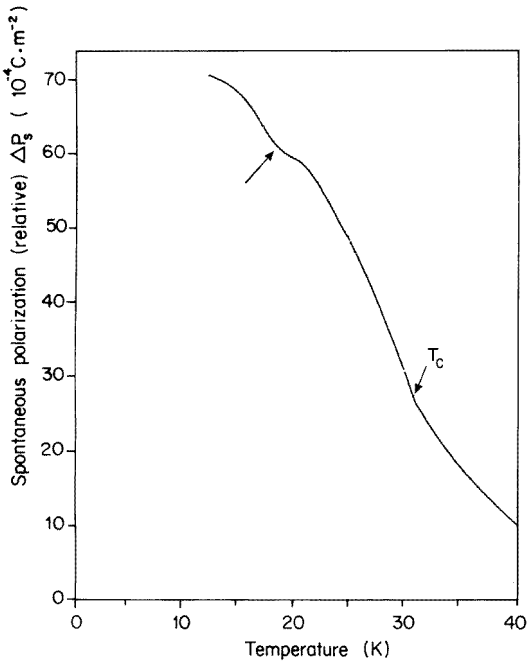

Figure 10. The variation of the spontaneous polarization of Fe–I boracite at low temperatures, indicating the magnetic phase transition at T_C and a spread dip between 15 and 20 K.

The detail of $\boldsymbol{P}_s(T)$ at low temperatures is shown in figure 10, where the onset of the magnetic ordering at $T_C = 30$ K is accompanied by a clear change of slope of the $\boldsymbol{P}_s(T)$ curve. The continuity of $\boldsymbol{P}_s$ at T_C indicates the second-order character of the magnetic phase transition, consistent with the results of the birefringence measurements [13]. The influence of the magnetic ordering on the temperature dependence of spontaneous polarization was also revealed in the magnetic orthorhombic phases of Cr–Cl [27], Ni–Br [28], Cu–Br [31] and Co–Br [26] boracites, and in the trigonal phase of Co–Cl [25, 26]. According to a Landau theory established for the magnetic phase transitions in boracite crystals [6], such an anomaly of $\boldsymbol{P}_s$ would indicate an influence of the magnetic transition on the crystal structure through the couplings between the order parameter or the magnetization components on the one hand, and the 'non-spontaneous' components of the polarization and strain (which already exist in the high-temperature paramagnetic phase) on the other hand.

Taking into account the magnetization-induced coupling effects (see table VI in reference [6]), the total polarization in the magnetic phase below T_C can be expressed as follows:

$$P_z = P_0 - \chi_0^E(\delta_1\eta_1^2 + \gamma_1\delta\eta_1 M_y)$$

where P_z stands for the spontaneous polarization along the unique c-axis, P_0 for the spontaneous polarization in the paramagnetic phase, χ_0^E for the electric susceptibility in the

parent $3m1'$ phase, η_1 for the component of the order parameter, M_y for the spontaneous magnetization along the monoclinic b-axis, and δ_1 and γ_1 for the coefficients of the Landau free energy which are temperature independent. The magnetization-induced polarization is described by the second term containing the low-temperature order parameters. Such a contribution would only modify the slope of the total polarization at T_C, as verified experimentally in figure 10. This indicates the purely magnetic character for the $3m1' \rightarrow m$ phase transition in Fe–I. A recent study of the magnetic structure of Co–Cl boracite by neutron powder diffraction [32] has revealed that the ferromagnetic monoclinic m phase is actually derived from the pseudo-parent paramagnetic $R3c1'$ phase, with a unit cell containing the same number of atoms as the trigonal cell and a magnetic Shubnikov group found by refinement to be Cc, while the ferroelectric/ferroelastic structure remains essentially trigonal below T_C. This structural model is in good agreement with the theoretical prediction [6].

In the ferromagnetic phase, a smooth but pronounced dip of the polarization appears in Fe–I crystals, spreading between 15 and 20 K (figure 10). Such an anomaly is also present in the slope of the temperature dependence of the magnetic birefringence of Fe–I, although no change in domain structure is visible to the naked eye [13]. The orthorhombic Cr–Cl boracite shows a similar behaviour both for the polarization and for the birefringence at low temperatures [27]. Measurements of the specific heat indicate a second anomaly for the Co–Cl, Co–Br and Co–I boracites below T_N (or T_C), which was attributed to a 'Schottky anomaly', the entropy of which is extracted from the total entropy: $\Delta_{Schottky} = \Delta_{Total} - \Delta_{Ordering}$ [33]. The temperature dependence of the magnetic neutron diffraction intensity of the orthorhombic Co–Br boracite also exhibits a change of slope associated with the 'Schottky anomaly'. The magnetic structure refinement shows that the onset of magnetic ordering in Co–Cl consists of a two-step process of the magnetic ordering, characterized below T_C by successive ordering of the three Co sites which display different magnetic moment values and orientations as well as different temperature behaviours, while the magnetic symmetry remains the same [34]. The 'Schottky anomaly' would result from the onset of ferromagnetism of Co(2) and Co(3), which are coupled antiferromagnetically. This ordering implies in the free-energy expression only changes in the entropy term, and thus is in agreement with the specific heat measurement. However, unlike for the Co boracites, the variation of the specific heat of Fe–I shows no measurable anomaly below $T_C = 31$ K [35].

6. Conclusions and remarks

The structural and magnetic phase transitions of Fe–I boracite have been studied by optical domain examination, dielectric characterization, and polarization measurements. The phase sequence and the transition temperatures, established by various techniques, can be summarized as follows:

$$\bar{4}3m1' \leftarrow T_1 \rightarrow mm21' \leftarrow T_2 \rightarrow m1' \leftarrow T_3 \rightarrow 3m1' \leftarrow T_C \rightarrow m$$

where $T_1 = 348$ and 348.5 K, $T_2 = 200$ and 202 K, $T_3 = 177$ and 187 K, $T_C = 31$ and 30.5 K, upon cooling and heating, respectively. The structural phase transitions have been demonstrated to have normal thermal hysteresis without evidence of an overlap of phases. The magnetic phase transition at T_C shows a small but reversed thermal hysteresis, probably due to the effect of magnetic domains near the phase transition.

The dielectric properties of Fe–I crystals indicate the first-order character of the structural phase transitions. The asymmetric spontaneous polarization in the trigonal phase for the

poling fields of opposite polarities along $\langle 111\rangle_{cub}$, qualitatively expected up to now [5], has been experimentally demonstrated here, in agreement with the symmetry properties of the species $\bar{4}3m1'F3m1'$ with non-reversible polar axes.

The phase transition at $T_C = 31$ K is purely of magnetic origin, but it has been shown to affect both the dielectric properties and the spontaneous polarization of Fe–I through magnetoelectric coupling terms. Note that this coupling is most certainly too weak to produce a simultaneous structural symmetry breaking during the magnetic ordering, as uniquely revealed in the case of Ni–I boracite [36, 37], but it is stronger than in the other magnetic boracites, giving rise to a splitting up of ferroelastic/ferromagnetic domains with unusually high linear spontaneous birefringence, associated with a structural distortion through an interaction of magnetostrictive type [13]. An investigation is in progress with a view to evaluating the values of the low-temperature-phase order parameters and the Landau free-energy coefficients [6] from the deviation of the spontaneous polarization below $T_C = 31$ K from the extrapolated line with the slope of $\boldsymbol{P}_s$ above T_C, by taking into account the new results on the magnetic structure [32] and the magnetic properties [38].

A remarkable anomaly of the spontaneous polarization appears in the ferromagnetic phase of Fe–I between 15 and 20 K, in agreement with the anomaly of the birefringence. These two anomalies are probably of magnetic origin, with spin reorientation. The specific heat, however, seems not to be sensitive to such a change in magnetic ordering in the case of Fe–I. Magnetic structure determinations by high-resolution neutron diffraction, and accurate susceptibility and magnetization measurements on ferroelastic/ferroelectric single-domain samples are needed to explain the origin of the low-temperature anomalies. It is also rewarding to study the linear and quadratic magnetoelectric effects which are *a fortiori* present in the magnetic phase of $Fe_3B_7O_{13}I$ crystals due to the evident ferromagnetic, ferroelectric and ferroelastic couplings.

Acknowledgments

This work was partly supported by the Fonds National Suisse de la Recherche Scientifique, and benefited from the technical help of Dr J-P Rivera, E Burkhardt, R Boutellier and R Cros.

References

[1] Schmid H 1994 *Ferroelectrics* **162** 317
[2] Schmid H 1969 *Growth Cryst.* **7** 25
[3] Nelmes R J and Thornley F R 1974 *J. Phys. C: Solid State Phys.* **7** 3840
[4] Schmid H and Tippmann H 1978 *Ferroelectrics* **20** 21
[5] Schmid H 1970 *Phys. Status Solidi* **37** 209
[6] Tolédano P, Schmid H, Clin M and Rivera J-P 1985 *Phys. Rev.* B **32** 6006
[7] Kobayashi J, Sato Y and Schmid H 1972 *Phys. Status Solidi* a **10** 259
[8] Schmid H and Trooster J M 1967 *Solid State Commun.* **5** 31
[9] Jagannathan R, Trooster J M and Viegers M P A 1973 *Int. J. Magn.* **4** 363
[10] Ye Z-G, Rivera J-P and Schmid H 1990 *Ferroelectrics* **106** 87
[11] Kovalev A V, Plakhtii V P, Bedrizova M N and Andreeva G T 1977 *Sov. Phys.–Solid State* **19** 1896
[12] Quézel G and Schmid H 1968 *Solid State Commun.* **6** 447
[13] Ye Z-G, Janner A-M, Rivera J-P and Schmid H 1993 *Ferroelectrics* **141** 135
[14] Schmid H, Chan P, Pétermann L A, Teufel F and Mändly M 1976 *Ferroelectrics* **13** 351
[15] Schmid H, Genequand P, Pouilly G and Chan P 1980 *Ferroelectrics* **25** 539
[16] Whatmore R W, Brierley C J and Ainger F W 1980 *Ferroelectrics* **27** 67
[17] Kobayashi J, Schmid H and Ascher E 1968 *Phys. Status Solidi* **26** 277

[18] Pétermann L A and Schmid H 1976 *Revue Phys. Appl.* **11** 49
[19] Kobayashi J and Mizutani I 1970 *Phys. Status Solidi* a **2** K89
[20] Kubel F and Janner A-M 1993 *Acta Crystallogr.* C **49** 657
Kubel F 1994 *Ferroelectrics* **160** 61
[21] Schmid H 1965 *J. Phys. Chem. Solids* **26** 973
[22] Schmid H and Tippmann H 1979 *J. Cryst. Growth* **46** 723
[23] Aizu K 1970 *Phys. Rev.* B **2** 754
[24] Rossignol J-F, Rivera J-P and Schmid H 1985 *Japan. J. Appl. Phys. Suppl.* **24** 574
[25] Mendoza-Alvarez M-E, Rivera J-P and Schmid H 1985 *Japan. J. Appl. Phys. Suppl.* **24** 1057
[26] Mendoza-Alvarez M 1985 *PhD Thesis* University of Geneva
[27] Ye Z-G, Rivera J-P, Burkhardt E and Schmid H 1991 *Phase Transitions* **36** 281
[28] Rivera J-P and Schmid H 1984 *Ferroelectrics* **55** 245
[29] Torre L P, Abrahams S C and Barns R L 1972 *Ferroelectrics* **4** 291
[30] Tolédano P, Schmid H, Clin M and Rivera J-P 1985 *Japan. J. Appl. Phys. Suppl.* **24** 347
[31] Berset G, Clin M, Rivera J-P and Schmid H 1988 *Ferroelectrics* **79** 177
[32] Schobinger-Papamantellos P, Ye Z-G, Schmid H, Ritter C and Suard E 1997 *Ferroelectrics* at press
[33] Clin M, Dai W, Gmelin E and Schmid H 1990 *Ferroelectrics* **108** 201
[34] Schobinger-Papamantellos P, Fischer P, Kubel F and Schmid H 1990 *Ferroelectrics* **108** 201
[35] Schnelle W, Crottaz O, Gmelin E and Schmid H 1997 to be published
[36] Ascher E, Rieder H, Schmid H and Stössel H 1966 *J. Appl. Phys.* **37** 1404
[37] Rivera J-P and Schmid H 1981 *Ferroelectrics* **36** 447
[38] Andreica D, Rivera J-P, Gentil S, Ye Z-G, Senthil Kumar M and Schmid H 1997 *Ferroelectrics* at press